Torsional behaviour of glass-joined, laser-processed Crofer 22 APU interconnect: Unravelling the effect of surface roughness on the shear strength

Ceramics International 48 (2022) 32837–32843

Contents lists available at ScienceDirect

Ceramics International

journal homepage: www.elsevier.com/locate/ceramint

Torsional behaviour of glass-joined, laser-processed Crofer 22 APU interconnect: Unravelling the effect of surface roughness on the shear strength

F. Smeacetto [a,*], E. Zanchi [a], D. Meena Narayana Menon [a], D. Janner [a], S. Lamnini [a], M. Salvo [a], S. De La Pierre [a], H. Javed [b], M. Ferraris [a,c]

[a] Politecnico di Torino, Department of Applied Science and Technology – DISAT, Corso Duca degli Abruzzi 24, 10129, Torino, Italy
[b] Sunfire GmbH, Gasanstaltstraße 2, 01237, Dresden, Germany
[c] J-TECH@PoliTO Advanced Joining Technologies, Italy

ARTICLE INFO

Keywords:
Joining
Torsion
Shear strength
Solid oxide cell
Laser
Surface modification

ABSTRACT

Glass-to-metal interfaces play a crucial role in the robustness and the mechanical integrity of solid oxide cells, and it is well known that a sound interface improves the mechanical reliability of the whole stack. The present work focuses on the torsional behaviour of hourglass-shaped Crofer 22 APU stainless steel joined by a glass sealant specifically designed for this application.

Specific focus was given to the Crofer surface modification by laser processing, namely, the laser fluence was varied to find suitable roughness parameters; a laser fluence of 14.1 J cm^{-2}, leading to a Crofer surface roughness of about 4.6 μm, was selected as the optimal Crofer surface processing before the joining process.

The torsional shear strength of glass-joined as-received Crofer was measured as 24 ± 7 MPa with mainly adhesive fracture mode, with failure jumping from one interface to the other, while the laser-processed Crofer gave 32 ± 5 MPa with cohesive failure. The approximate 30% increase of torsional shear strength is due to the mechanical interlocking effect given by glass infiltration inside the laser-induced protrusions on Crofer as evidenced by SEM/EDS on cross-sections and fracture surfaces after torsion tests.

1. Introduction

Efficient electrochemical energy conversion in solid oxide cells (SOC) can be achieved only by a reliable integration and joining technology. The metallic interconnect must be joined and sealed to the adjacent ceramics components to produce a SOC stack [1,2]. The sealing procedure, and consequently the reliability of the whole joined parts, presents significant challenges because the robustness of different interfaces is a key parameter to preventing gas mixing and consequent stack failure.

One of the major challenges is to assess the proper sealing material and the related interface with adjacent materials, taking into consideration different stress conditions present in SOC stacks [3,4]. Glass-based sealings, characterized by different properties according to their composition, play a crucial role in the SOC performance and durability [5–9]: as an example, rising the internal stack operating pressure by pressurised electrolysis would provide an efficient solution for the delivery of pressurised hydrogen at a reduced cost [10], but it is unquestionably linked to the availability of a mechanically strong glass-to-interconnect bond.

Although glass-to-metallic interconnects bond has received considerable and critical attention in the past, most of the work has been devoted to evaluating tensile or bending strength [11,12] while, under relevant SOC operating conditions, the glass-based sealant is also and foremost exposed to shear stresses.

To the best of the authors' knowledge, only a limited number of studies exist on the shear strength evaluation of joined components for solid oxide cells [13–17].

The torsion test on hourglass-shaped samples is recognised as one of the most suitable and reliable methods to measure the "pure" shear strength of glass-to-metal joints, without additional stresses such as bending or peeling as it happens with other tests which provide

* Corresponding author.
E-mail address: federico.smeacetto@polito.it (F. Smeacetto).
URL: https://www.j-tech.polito.it/ (M. Ferraris).

https://doi.org/10.1016/j.ceramint.2022.07.210
Received 9 June 2022; Received in revised form 13 July 2022; Accepted 18 July 2022
Available online 31 July 2022

"apparent" and size-dependent shear strength values [18]. Furthermore, it has also been demonstrated that torsion tests are suitable for obtaining size-independent pure shear strength results. The shape of torsion curves may be used to detect a cohesive or adhesive fracture in a glass-to-metal joint [19].

To obtain a cohesive fracture, and thus fully exploit the joining material's mechanical strength, several surface treatments are usually done before joining similar or dissimilar materials (i.e. polymer-to-metal, ceramic-to-glass, polymer-to-polymer, etc …) [20–22]. As an example in the field of SOC applications, Ritucci et al. [23] investigated the mechanical adhesion of joints made of a diopside based glass-ceramic (labelled as V11) and Crofer interconnects after three different surface treatments: the adhesion was evaluated by measuring the fracture energy, but without mentioning how the surface roughness influenced the glass-to-metal adhesion.

A suitable metal roughness is needed to fully exploit the mechanical interlocking effect in a glass-to-metal joint. This paper aims to investigate, for the first time, the effect of Crofer 22 APU stainless-steel surface modification by a fibre laser and to measure it by torsion tests on glass-joined samples. The results of this work will provide SOC designers with a reliable set of torsional shear strength values, showing the proper balance of an adequate design of the interconnect roughness while avoiding large defects at the glass-to-metal interface.

2. Experimental

As-received Crofer 22 APU (in the following abbreviated as "Crofer") hourglass samples (THG-25, 25 mm diameter, size and shape reported in Ref. [19]) were mechanically polished to obtain an average surface roughness $S_a = 250$ nm, measured by profilometry specified below. The samples were then cleaned for 5 min in an ultrasonic bath with acetone, rinsed with ethanol, and air-dried before laser processing.

An Infrared Nanosecond fibre laser (wavelength = 1064 nm, pulse width = 12 ns, spot size = 60 μm) was focused onto the steel at normal incidence for surface modification. Laser parameters such as scan speed (5 mm/s), pulse repetition rate (25 kHz), and lateral scan spacing (40 μm) were fixed while the average laser power was varied. In such a way, it was possible to adjust the average surface roughness (Sa) and the maximum peak to valley height (Sz) of the steel surface in a controllable manner. After each laser modification and before further processing, Crofer samples were sonicated in acetone and ethanol solutions for 5 min each to remove any eventual residue that might have formed on the surface during laser processing. The surface morphology of the samples was analysed via a stylus profilometer (Form Talysurf Intratouch, Taylor Hobson, USA). A selected surface area of 0.75 mm^2 (1.5 mm × 0.5 mm) was scanned, and the physical parameters of the surface in terms of surface roughness (Sa, Sz) were derived.

The compositional modification of laser treatment on the Crofer surface was investigated by a Bruker D8 diffractometer with Cu-Kα radiation. Diffraction patterns were recorded at room temperature in a 2Theta range of 10°–70°, with a step size of 0.013° 2Theta and mean-time per step of 100 s; recorded patterns were analysed using Pan-Alytical X'Pert software and PDF-2 database.

A silica-based, boron-containing glass-based sealant (proprietary composition) with composition and properties similar to those reported in Ref. [24] was used as the sealing material.

For the joining process, glass powder was mixed with a minimum amount of ethanol and the obtained slurry was manually deposited on a one-half hourglass; a specific sample holder was designed to obtain a 200–250 μm thick slurry layer.

Afterwards, the second half hourglass was positioned on top of the previous one and the joining process was carried out in a Carbolite 1800 HTF furnace operating in air, without applying any pressure, just an alumina sample holder was used to keep the samples in place.

To choose the optimal conditions, several laser-processed Crofer hourglasses were joined by the glass-based sealing material at 900–950 °C, in air, with a joining process of about 2 h.

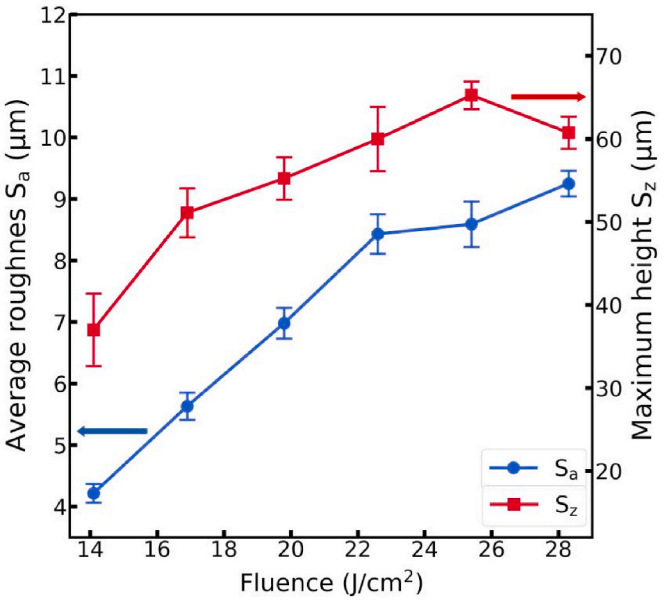

Fig. 1. Variation of average roughness (Sa) and maximum peak to valley height (Sz) *versus* laser fluence.

Both as-received and laser-processed hourglass joined samples were produced.

Torsion tests were performed with a Testresources custom made machine (160-GT585 Testresources, USA): joined samples were placed in 30 mm × 30 mm grips to hold them during the test. Then a preload of 5 Nm was set with a constant test speed of 1 deg/min. After the preload, a constant speed of 5 deg/min was set for testing. The test stopped when a fracture was detected.

Morphological characterization of as-joined and post-mortem samples was done by using a field-emission scanning electron microscope (FESEM; SupraTM 40, Zeiss, Oberko-chen, Germany) equipped with an energy dispersive X-ray analyser (EDS, Bruker, Germany). To observe the cross-sections, hourglass samples were embedded in epoxy resin and polished up to 4000 SiC paper.

3. Results and discussion

3.1. Surface characterization of laser-processed Crofer

3.1.1. Surface roughness

Laser pulse interaction with a metallic surface can deliver a large amount of energy over a very short time scale, e.g., nanoseconds. If the laser energy is above a given threshold, the part absorbed by the target material results in instantaneous melting and eventual material vaporization at the laser focus and nearby regions [25]. Upon reaching the vaporization temperature, a substantial increase in material removal in the form of vapour and molten liquid droplets occurs. This phenomenon is known as phase explosion. In this work, the employed working energy is well beyond the phase explosion threshold observed with metals (<10 J cm^{-2}) [26,27].

Working in the phase explosion regime allows removing material fast and in a controlled way. Consequently, the final surface morphology results mainly from material removal via vaporization, rapid condensation of molten material, and redeposition of ejected material as micro-/nano-particles on the surface. The controllable laser parameters influencing surface features are average laser power, scan speed, scan line spacing, and pulse repetition rate. In this study, however, the main parameter of interest is laser fluence (F) given by:

Table 1
Laser parameters and surface roughness values on Crofer.

Fluence (J · cm^{-2})	Sa (μm)	Sz (μm)
14.1	4.6	39.7
28.3	8.8	61.6

$$F = \frac{Pulse\ energy}{\pi \cdot \left(\frac{w_0}{2}\right)^2}$$

where w_0 represents focal spot size diameter (60 μm) and *Pulse energy* is given by:

$$Pulse\ energy = \frac{P_{avg}}{PRR}$$

where P_{avg} is the average laser power and *PRR* is the pulse repetition rate. Fluence includes the pulse repetition rate, scan speed, and average power since it represents the amount of energy per unit area integrated over time. The variation of surface roughness parameters with laser fluence was first characterized as follows: Fig. 1 shows the average roughness (Sa) and maximum peak to valley height of surface roughness (Sz) achievable upon variation of laser fluence. Both roughness parameters (Sa and Sz) increase with laser fluence due to larger pulse energy.

A pair of low-high average roughness (Sa) values were chosen for the tests to select the best candidate for SOC joining application. Table 1 reports the laser parameters selected and the obtained surface roughness for the joining strength tests. The Profilometer 3D surface mapping in Fig. 2 clearly presents the effect on the surface morphology introduced by laser processing. The (Sã4.6 μm) profilometer 3D map in Fig. 2a distinctly shows the laser scan lines as valley regions with side peaks for the low roughness sample. For this process, the spatial distribution is more uniform than the one with the higher roughness sample (Sã8.8 μm), as reported in Fig. 2b. Indeed, for the high roughness, the excessive energy has resulted in melt and redeposition generating a relatively random peak distribution.

3.1.2. Surface characterization

Crofer is usually subjected to oxidation in air, to form a controlled oxide scale before or during joining. To evaluate the laser effect on the oxide scale formation, both laser-processed and as-received Crofer samples were subjected to oxidation in air at T > 900 °C for 2 h, which is the thermal treatment used for the joining process, as will be discussed in the following section. Recorded XRD patterns for laser-processed non-oxidized Crofer are reported in Fig. 3b for comparison purposes, together with results for oxidized Crofer in Fig. 3a and laser-processed and oxidized Crofer in Fig. 3c. It is evident that the laser caused partial oxidation of the steel substrate, as revealed by the presence of a Fe and Cr rich oxide scale, identified with the Cr_2FeO_4 phase in the PDF-2 database.

As expected, the thermally grown oxide scale formed on oxidized Crofer in Fig. 3b consists of $MnCr_2O_4$ spinel as the main phase and Cr_2O_3 as the second phase. This evidence is in agreement with the study published by Talic et al. [28], where the Crofer pre-oxidation treatment is investigated at different temperatures and atmospheres. On the other hand, laser-processed Crofer after oxidation in Fig. 3c confirms the presence of a mixed Cr–Fe oxide scale as the main phase, matching with $Cr_{1.3}Fe_{0.7}O_3$ (code 035–1112 in PDF-2), with the main peaks of chromia also identified. It is interesting to note that no $MnCr_2O_4$ spinel is formed on laser-processed Crofer after oxidation, but a $Cr_{1.3}Fe_{0.7}O_3$ scale: it is thus clear that this laser treatment could influence the oxidation behaviour of the Crofer substrate. Although the long-term stability of the $Cr_{1.3}Fe_{0.7}O_3$ scale during SOC working conditions, and in contact with the sealant has still to be assessed, this new oxidation behaviour might be of interest and will be the subject of further investigation.

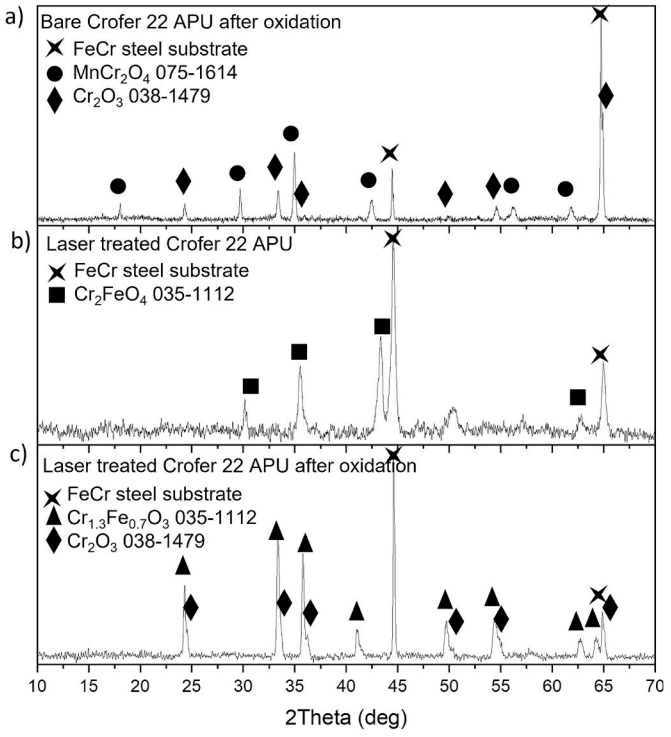

Fig. 3. XRD patterns of bare Crofer after oxidation (a) laser-processed Crofer(b) and laser-processed Crofer after oxidation treatment (c).

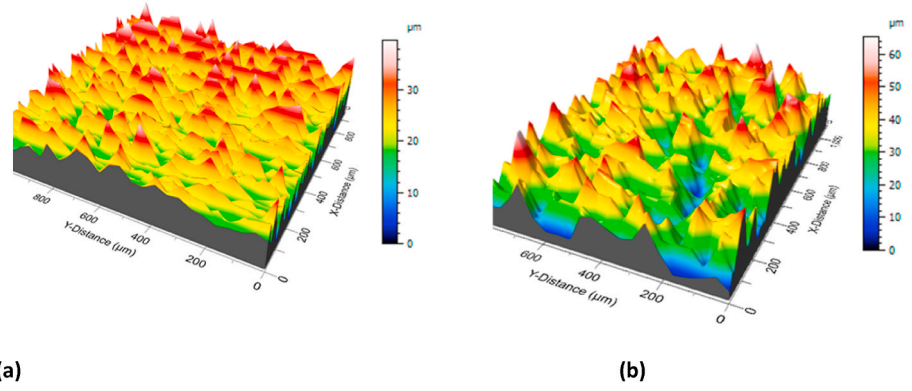

(a) (b)

Fig. 2. Profilometer surface map for chosen laser parameters with average surface roughness (a) 4.6 μm and (b) 8.8 μm.

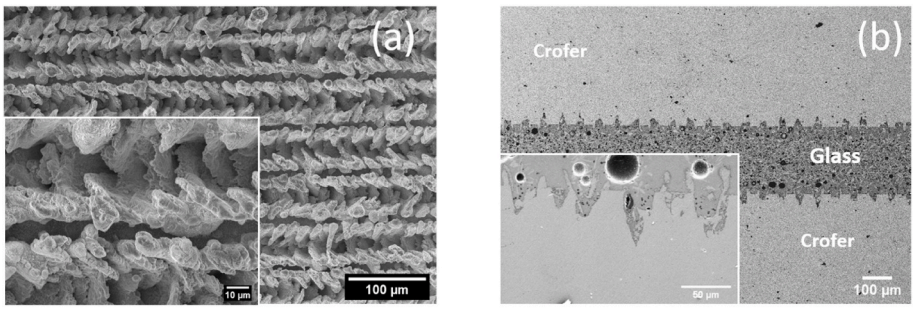

Fig. 4. SEM top view of the laser-processed Crofer surfaces by using the two above mentioned laser process parameters, laser fluency of 14.1 J cm^{-2} (a) and the corresponding joined samples cross-section (b) before the torsion test.

3.2. Morphological and mechanical characterization of joined samples

Fig. 4 shows the SEM top view of the laser-processed Crofer surfaces by using the two above mentioned laser parameters (Fig. 4a, c) and the corresponding joined samples cross-sections (Fig. 4b, d).

It is evident that the roughness is substantially different in the two cases (Fig. 4a and c) and that the Crofer surface morphology changes as a function of increased laser fluence. A periodic patterned and ordered arrangement showing a wave-like surface was obtained with the laser fluence of 14.1 J cm^{-2}, as shown in Fig. 4a. Further increasing the laser fluence to 28,3 J cm^{-2} resulted in an irregular pattern of the surface roughness, with the texture characterized by important changes, (reported in supplementary material information), with several not uniform surface protrusions.

Fig. 4b showed the SEM cross-section of the joined samples, concerning the Crofer surface modification with a laser fluence of 14.1 J cm^{-2}, before the torsion test.

A perfect glass infiltration was obtained for the lower laser fluence (Fig. 4b): the glass appears to be tightly bonded with the Crofer and no significant defects were identified at the interface.

On the contrary, an irregular surface modification occurred in the case of high laser fluence, as reported in supplementary material information with a consequent partial infiltration into the Crofer protrusions and some porosity evident in the sealant Based on these preliminary observations, a fluence of 14.1 J cm^{-2} was selected for laser-processed Crofer substrates to be joined and tested in torsion.

This specific hourglass geometry, labelled as THG (Torsion Hour Glass), was previously modelled and experimentally verified in different laboratories, and it is considered one of the very few appropriate methods to measure the shear strength under torsional loading for a

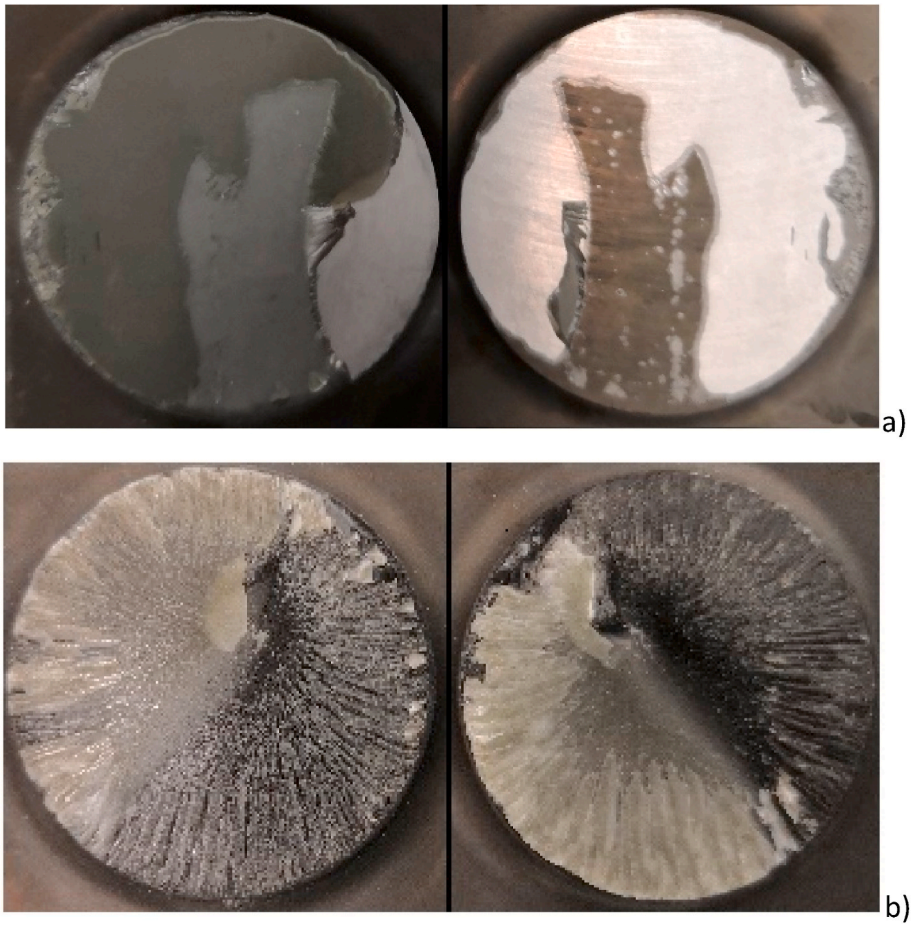

Fig. 5. Visual appearance of typical fracture surfaces after torsion test, for as-received (a) and laser-processed (b) joined samples.

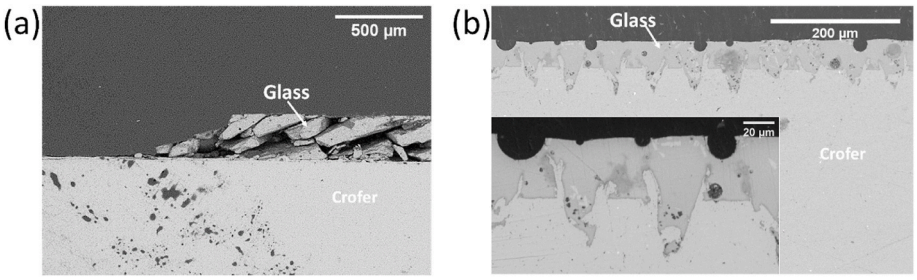

Fig. 6. Typical cross-sections of steel/glass interfaces in joined samples after torsion tests: as-received Crofer (a) and laser-processed Crofer (b).

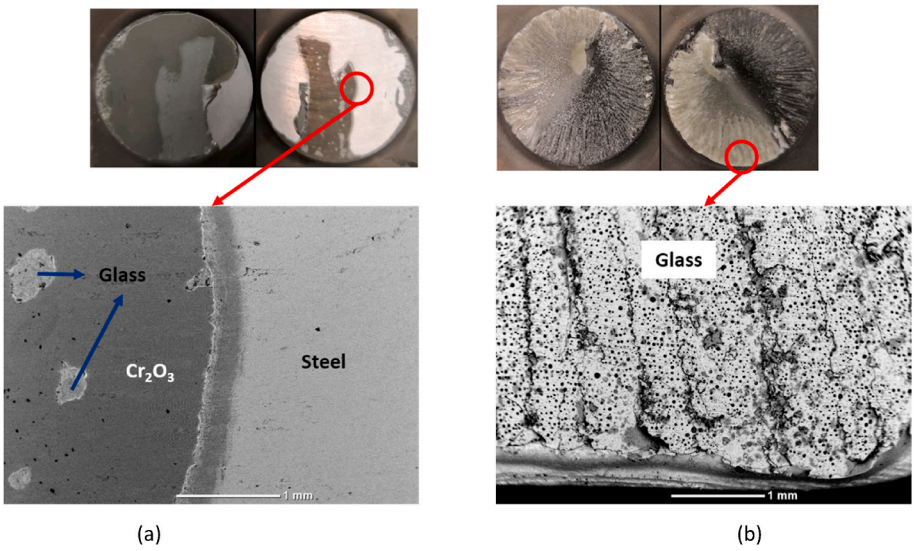

Fig. 7. SEM on fracture surfaces after torsion test and detected materials by EDS analysis for as-received (a) and laser-processed (b) joined samples. Glass is partially present on both surfaces in a typical mainly adhesive (with failure jumping from one interface to the other) fracture mode in (a) for as-received joined samples; a completely different fracture surface with glass present on both surfaces and glass infiltrating the laser-processed Crofer surface is evident in (b) for laser-processed joined samples (inset: samples' visual appearance).

wide variety of joined samples [29].

The role of brittle or ductile joining materials on torsion results, together with the fracture propagation has been reported in previous works [30]. In this work, the glass-based joining material at room temperature is characterized by an intrinsically brittle nature, with a linear behaviour until fracture during torsion tests; furthermore, all samples exhibited the fracture in the joined region. With both these requirements fulfilled, the maximum torque of the torsion test can be used to calculate the shear strength of the joined samples, according to eqs. (1) and (2):

$$\tau_{max} = Shear\ Strenght = \frac{M_{max} \cdot R_e}{J} \quad \text{Eq. 1}$$

with:

$$J = \frac{\pi R_e^4}{2} \quad \text{Eq. 2}$$

where τ_{max} is the shear strength, $M_{max\ is}$ the maximum torque, J is the polar moment of inertia and R_e is the radius of the joined area.

The shear strength of the as-received glass-joined Crofer-samples was 24 ± 7 MPa, while the laser-processed Crofer, with an average surface roughness of 8.8 μm, gave a shear strength of 32 ± 5 MPa.

The typical fracture surfaces after the torsion test for as-received (a) and laser-processed (b) hourglass samples are shown in Fig. 5, where the different failure behaviour is compared. Their visual appearance evidences a major difference in the fracture mode: glass is partially present on both surfaces in a typical mixed fracture mode in Fig. 5a for as-received joined samples. A completely different fracture surface is evident in Fig. 5b for laser-processed joined samples: the fracture is

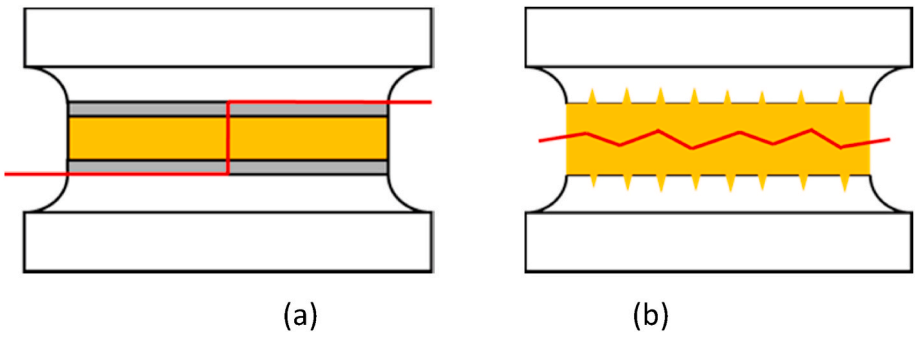

Fig. 8. Sketch of the typical fracture propagation mode for the as-received Crofer joined samples (a) and for laser-processed Crofer joined samples (b).

mainly propagating through the sealant, in a cohesive mode, with glass present on both fracture surfaces.

Fig. 6 shows the typical cross-sections of Crofer/glass interfaces in joined samples after torsion tests: as-received steel (a) and laser-processed steel (b). The approximate 30% increase in torsional shear strength is due to the mechanical interlocking effect given by glass infiltration inside the laser-induced protrusions on Crofer and it was evidenced by SEM/EDS on cross-sections after the torsion tests.

What is evidenced in Fig. 7b, (fracture surface top view of the glass-joined laser-processed Crofer after torsion test) is a further confirmation of what was already pointed out by observing the cross-section after testing (Fig. 6b) of the same sample, where the glass-steel interface is continuous and crack free.

The EDS analysis results are shown in Fig. 7 by arrows, indicating the presence of Crofer, chromium oxide and glass elements in large areas of the fracture surfaces after torsion tests, thus confirming the mixed-mode fracture (Fig. 7a); on the contrary, the glass debris found on both surfaces in Fig. 8b confirms the cohesive behaviour for laser-processed Crofer joined samples.

As a summary, Fig. 8a is a sketch of the typical fracture propagation mode for the as-received Crofer joined samples, showing the mainly adhesive mode, with failure jumping from one interface to the other, failure of these joints, while Fig. 8b sketches the fracture propagation mode for laser-processed Crofer joined samples, showing the cohesive behaviour for this type of joints.

4. Conclusions

This work evidenced some interesting aspects of the torsional behaviour of hourglass-shaped Crofer 22 APU joined by a glass specifically designed for solid oxide cell stacks.

Specific focus was given to Crofer surface modification by laser processing and laser fluence of 14.1 J cm^{-2}, leading to a Crofer surface roughness of about 4.6 μm, which was selected as the optimal surface processing condition before the joining process.

The torsional shear strength of glass-joined as-received Crofer was measured as 24 ± 7 MPa with a mainly adhesive failure mode, while the laser-processed Crofer gave 32 ± 5 MPa with cohesive failure and the laser formed Crofer protrusions infiltrated by the glass.

The approximate 30% increase in torsional shear strength is due to the mechanical interlocking effect given by glass infiltration inside the laser-induced protrusions, as clearly demonstrated by the SEM analyses on the as joined cross-sections and the fracture surfaces after torsion tests.

Declaration of competing interest

The authors declare that they have no known competing financial interests or personal relationships that could have appeared to influence the work reported in this paper.

Acknowledgements

The experimental activity of MSc Gabriele Sanfratello is kindly acknowledged.

The research leading to this work received funding from European Commission's Fuel Cells Hydrogen Joint Undertaking (FCH 2 JU), grant agreement No. 874577 – NewSOC.

Torsion tests have been done by Gabriele Sanfratello during his Energy Engineering Master Degree Stage at J-TECH@PoliTO labs (https://www.j-tech.polito.it/).

Appendix A. Supplementary data

Supplementary data to this article can be found online at https://doi.org/10.1016/j.ceramint.2022.07.210.

References

[1] J.W. Fergus, Metallic interconnects for solid oxide fuel cells, Mater. Sci. Eng. 397 (2005) 271–283, https://doi.org/10.1016/j.msea.2005.02.047.
[2] J. Wu, X. Liu, Recent development of SOFC metallic interconnect, J. Mater. Sci. Technol. 26 (2010) 293–305, https://doi.org/10.1016/S1005-0302(10)60049-7.
[3] M. Peksen, A. Al-Masri, L. Blum, D. Stolten, 3D transient thermomechanical behaviour of a full scale SOFC short stack, Int. J. Hydrogen Energy 38 (2013) 4099–4107, https://doi.org/10.1016/j.ijhydene.2013.01.072.
[4] W. Jiang, Y.C. Zhang, W.Y. Zhang, Y. Luo, W. Woo, S.T. Tu, Growth and residual stresses in the bonded compliant seal of planar solid oxide fuel cell: thickness design of window frame, Mater. Des. 93 (2016) 53–62, https://doi.org/10.1016/j.matdes.2015.12.145.
[5] H. Lee, U.S. Kim, S.D. Kim, S.K. Woo, W.J. Chung, SiO2–B2O3-BaO-WO3 glasses with varying Al2O3 content as a sealing material for reversible solid oxide fuel cells, Ceram. Int. 46 (2020) 18256–18261, https://doi.org/10.1016/j.ceramint.2020.04.148.
[6] H. Javed, K. Herbrig, A.G. Sabato, D. Ferrero, M. Santarelli, C. Walter, F. Smeacetto, Electrical characterization of glass-ceramic sealant-metallic interconnect joined samples under solid oxide electrolysis cell conditions; influence on the microstructure and composition at the different polarized interfaces, Ceram. Int. 47 (2021) 8184–8190, https://doi.org/10.1016/j.ceramint.2020.11.176.
[7] Y.-S. Chou, J.W. Stevenson, P. Singh, Effect of aluminizing of Cr-containing ferritic alloys on the seal strength of a novel high-temperature solid oxide fuel cell sealing glass, J. Power Sources 185 (2008) 1001–1008, https://doi.org/10.1016/j.jpowsour.2008.09.004.
[8] S.R. Choi, N.P. Bansal, A. Garg, Mechanical and microstructural characterization of boron nitride nanotubes-reinforced SOFC seal glass composite, Mater. Sci. Eng. (2007) 509–515, https://doi.org/10.1016/j.msea.2007.01.084, 460–461.
[9] F. Heydari, A. Maghsoudipour, Z. Hamnabard, S. Farhangdoust, Mechanical properties and microstructure characterization of zirconia nanoparticles glass composites for SOFC sealant, Mater. Sci. Eng. 552 (2012) 119–124, https://doi.org/10.1016/j.msea.2012.05.019.
[10] A. Hagen, R. Caldogno, F. Capotondo, X. Sun, Metal supported electrolysis cells, Energies 15 (2022) 2045, https://doi.org/10.3390/en15062045.
[11] C.-K. Lin, T.-W. Lin, S.-H. Wu, W.-H. Shiu, C.-K. Liu, R.-Y. Lee, Creep rupture of the joint between a glass-ceramic sealant and lanthanum strontium manganite-coated ferritic stainless steel interconnect for solid oxide fuel cells, J. Eur. Ceram. Soc. 38 (2018) 2417–2429, https://doi.org/10.1016/j.jeurceramsoc.2018.01.016.
[12] S. Rodríguez-López, J. Wei, K.C. Laurenti, I. Mathias, V.M. Justo, F.C. Serbena, C. Baudín, J. Malzbender, M.J. Pascual, Mechanical properties of solid oxide fuel cell glass-ceramic sealants in the system BaO/SrO-MgO-B 2 O 3 -SiO 2, J. Eur. Ceram. Soc. 37 (2017) 3579–3594, https://doi.org/10.1016/j.jeurceramsoc.2017.03.054.
[13] J. Malzbender, J. Mönch, R.W. Steinbrech, T. Koppitz, S.M. Gross, J. Remmel, Symmetric shear test of glass-ceramic sealants at SOFC operation temperature, J. Mater. Sci. 42 (2007) 6297–6301, https://doi.org/10.1007/s10853-006-1178-1.
[14] F. Smeacetto, A. De Miranda, A. Ventrella, M. Salvo, M. Ferraris, Shear strength tests of glass ceramic sealant for solid oxide fuel cells applications, Adv. Appl. Ceram. 114 (2015) S70–S75, https://doi.org/10.1179/1743676115Y.0000000042.
[15] T. Osipova, J. Wei, G. Pećanac, J. Malzbender, Room and elevated temperature shear strength of sealants for solid oxide fuel cells, Ceram. Int. 42 (2016) 12932–12936, https://doi.org/10.1016/j.ceramint.2016.05.064.
[16] M. Fakouri Hasanabadi, M.A. Faghihi-Sani, A.H. Kokabi, J. Malzbender, The analysis of torsional shear strength test of sealants for solid oxide fuel cells, Ceram, Bar Int. 43 (2017) 12546–12550, https://doi.org/10.1016/j.ceramint.2017.06.128.
[17] M. Fakouri Hasanabadi, A.H. Kokabi, M.A. Faghihi-Sani, S.M. Groß-Barsnick, J. Malzbender, Room- and high-temperature torsional shear strength of solid oxide fuel/electrolysis cell sealing material, Ceram. Int. 45 (2019) 2219–2225, https://doi.org/10.1016/j.ceramint.2018.10.134.
[18] S. De La Pierre, T. Scalici, P. Tatarko, A. Valenza, L. Goglio, D.S. Paolino, M. Ferraris, Torsional shear strength and elastic properties of adhesively bonded glass-to-steel components, Mater. Des. 192 (2020), 108739, https://doi.org/10.1016/j.matdes.2020.108739.
[19] M. Ferraris, S. De la Pierre, A.G. Sabato, F. Smeacetto, H. Javed, C. Walter, J. Malzbender, Torsional shear strength behavior of advanced glass-ceramic sealants for SOFC/SOEC applications, J. Eur. Ceram. Soc. 40 (2020) 4067–4075, https://doi.org/10.1016/j.jeurceramsoc.2020.04.034.
[20] L. Novák, L. Fojtl, M. Kadlečková, L. Mañas, I. Smolková, L. Musilová, A. Minařík, A. Mráček, T. Sedláček, P. Smolka, Surface modification of metallic inserts for Enhancing adhesion at the metal–polymer interface, Polymers (Basel) 13 (2021) 4015, https://doi.org/10.3390/polym13224015.
[21] V. Casalegno, M. Ferraris, S. Perero, M. Suess, C. Wilhelmi, M. Pedroni, E. Vassallo, M. Salvo, A plasma pre-treatment to improve adhesion on SiC and Si3N4 ceramics, Mater. Lett. 272 (2020) 127855, https://doi.org/10.1016/j.matlet.2020.127855.
[22] G. Peralta Marino, S. De la Pierre, M. Salvo, A. Díaz Lantada, M. Ferraris, Modelling, additive layer manufacturing and testing of interlocking structures for joined components, Sci. Rep 12 (2022) 2526, https://doi.org/10.1038/s41598-022-06521-z.
[23] I. Ritucci, R. Kiebach, B. Talic, L. Han, P. Zielke, P.V. Hendriksen, H.L. Frandsen, Improving the interface adherence at sealings in solid oxide cell stacks, J. Mater. Res. 34 (2019) 1167–1178, https://doi.org/10.1557/jmr.2018.459.
[24] H. Javed, A.G. Sabato, M. Mansourkiaei, D. Ferrero, M. Santarelli, K. Herbrig, C. Walter, F. Smeacetto, Glass-ceramic sealants for SOEC: thermal characterization

and Electrical resistivity in dual atmosphere, Energies 13 (2020) 3682, https://doi.org/10.3390/en13143682.
[25] D. Marla, U.V. Bhandarkar, S.S. Joshi, Modeling nanosecond pulsed laser ablation: a focus on temperature dependence of material properties,, Manuf. Lett. 2 (2014) 13–16, https://doi.org/10.1016/j.mfglet.2013.12.001.
[26] C. Porneala, D.A. Willis, Observation of nanosecond laser-induced phase explosion in aluminum, Appl. Phys. Lett. 89 (2006) 211121, https://doi.org/10.1063/1.2393158.
[27] X. Xu, Phase explosion and its time lag in nanosecond laser ablation, Appl. Surf. Sci. (2002) 197–198, https://doi.org/10.1016/S0169-4332(02)00304–00305, 61–66.
[28] B. Talic, S. Molin, P.V. Hendriksen, H.L. Lein, Effect of pre-oxidation on the oxidation resistance of Crofer 22 APU, Corrosion Sci. 138 (2018) 189–199, https://doi.org/10.1016/j.corsci.2018.04.016.
[29] M. Ferraris, A. Ventrella, M. Salvo, Y. Katoh, D. Gross, Torsional shear strength tests for glass-ceramic joined silicon carbide, Int. J. Appl. Ceram. Technol. 12 (2015) 693–699, https://doi.org/10.1111/ijac.12248.
[30] M. Ferraris, M. Salvo, V. Casalegno, S. De La Pierre, L. Goglio, A. Benelli, Torsion test vs. Other methods to obtain the shear strength of elastic-plastic adhesives, Appl. Sci. 12 (2022) 3284, https://doi.org/10.3390/app12073284.